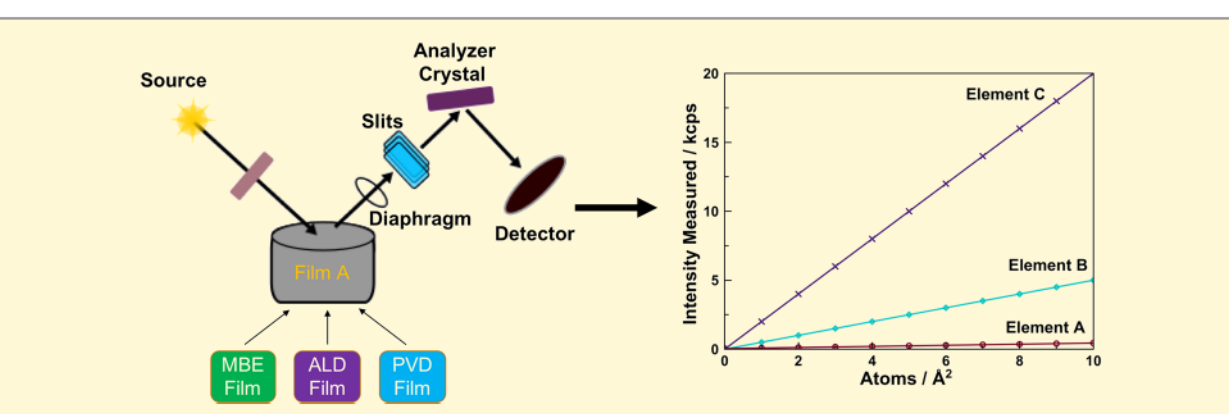
Sub-Monolayer Accuracy in Determining the Number of Atoms per Unit Area in Ultrathin Films Using X-ray Fluorescence

Danielle M. Hamann, Dylan Bardgett, Dmitri Leo M. Cordova, Liese A. Maynard, Erik C. Hadland, Alexander C. Lygo, Suzannah R. Wood, Marco Esters, and David C. Johnson

Department of Chemistry, Materials Science Institute, University of Oregon, Eugene, Oregon 97403, United States

Supporting Information

Downloaded by UNIV OF OREGON at 14:29:42:567 on July 02, 2019 from https://pubs.acs.org/doi/10.1021/acs.chemmater.8b02591.



ABSTRACT: The composition and thickness of thin films determine their physical properties, making the ability to measure the number of atoms of different elements in films both technologically and scientifically important. For thin films, below a certain thickness, the X-ray fluorescence intensity of an element is proportional to the number of atoms. Converting this intensity to the number of atoms per unit area is challenging due to experimental geometries and other correction factors. Hence, the ratio of intensities is more commonly used to determine the composition in terms of element ratios using standards or a model. Here, the number of atoms per unit area was determined using X-ray structure information for over 20 different crystallographically aligned samples with integral unit cell thicknesses. The proportionality constant between intensity and the number of atoms per unit area was determined from linear fits of the background subtracted X-ray fluorescence intensity plotted versus the calculated number of atoms per unit area for each element. The results demonstrate that X-ray fluorescence is very sensitive, capable of measuring changes in the number of atoms of less than 1% of a monolayer for some elements in a variety of sample matrices. Using the calibrated values, an 8 unit cell thick MoSe₂ was grown and characterized, demonstrating the usefulness of the ablity to quantify the number of atoms per unit area in a film.

The discovery that isolated two-dimensional layers have extraordinary properties that are not found in their bulk counterparts has resulted in intense experimental and theoretical interest in these materials.

A distinct challenge toward the future use of these materials in new technologies is developing techniques to grow single layers of various 2D solids over large areas. While a variety of techniques have been explored to prepare monolayers, chemical vapor deposition involving a volatile metal source has become increasingly popular. ^{13–26} Typically, "about a monolayer" of a metal is deposited on a surface and treated at high temperatures with a second reagent to form domains of the desired monolayer on substrates. 27-29 Since the deposited metal species is typically not volatile, once the precursor has reacted on the surface, time is the parameter that is tuned to achieve a monolayer of coverage. This type of monolayer synthesis creates an analytical need to quickly measure fractional monolayer amounts of elements on a substrate, ideally without significant sample preparation.

More generally, measuring the number of atoms per unit area of each element in a thin film is a challenging analytical problem and critically important in many situations. Physical properties depend on both composition and thickness of constituent layers in devices, and the properties of compound films are a sensitive function of composition. A variety of approaches have been used to determine composition, including Rutherford backscattering, electron probe microanalysis, particle-induced X-ray emission, X-ray photoelectron spectroscopy, time-of-flight secondary ion mass spectrometry, and a variety of electron microscopy techniques. ^{2,7} –30 Most of these techniques involve expensive instrumentation, and several also require significant sample preparation. Sensitivity and converting the signal to the number of atoms of each element per unit area can also be very challenging, particularly

Received: June 19, 2018 Revised: August 15, 2018 Published: August 16, 2018



if the signal is sensitive to the matrix. Typically, only a composition ratio is determined, as taking the ratio of two different elements eliminates several difficult to determine proportionality factors that depend on geometry, other instrument dependent factors, and the sample itself.

X-ray fluorescence (XRF) is a metrology method that can determine both composition and thickness of thin films and has several advantages. While it requires absorption corrections (via standards with similar matrices or modeling) and the usre of standards to obtain instrument parameters, it is quick and precise. Early work on the XRF analysis of thin films focused on using a variety of different methods to correct for absorption effects in the thin film geometry. 31,32 This led to the development of XRF as a tool to characterize relatively simple multilayer films in the advance of materials for a variety of applications, including memory devices and optical recording.33,34 More recent reports have shown that XRF is also a useful approach to characterize patterned thin films, with intensity differences before and after patterning proportional to the amount of material removed during the patterning process.³⁵ While a significant challenge has been to accurately correct the XRF data for absorption effects, there is at least one report where XRF using wavelength-dispersive X-ray detection was used to examine films that are thin enough that absorption could be ignored.³⁶ This study showed that a resolvable composition difference of 0.025 atomic percent could be obtained with relatively short counting times in a series of chalcopyrite solar cells.

In this paper, we present data showing that XRF intensity is proportional to the number of atoms per unit area in ultrathin films and the intensity is relatively insensitive to the matrix. The number of atoms per unit area for a subset of exceptionally smooth films was calculated using data from a combination of X-ray reflectivity, specular diffraction, and inplane diffraction scans. Calculating the proportionality constant between XRF intensity and the number of atoms per unit area simply requires division of the measured XRF intensity by the calculated number of atoms per unit area. The proportionality constant in over 20 samples with a range of thicknesses is consistent for the elements examined, indicating this is a valid approach. Once the proportionality constant is known for an element, preparing films of known compounds with defined atomic ratios between the previously studied element and other elements enables the determination of the proportionality constant for previously unstudied elements without the need for exceptionally smooth films. The consistency of results for films containing a wide range of different matrix constituents makes this a simple, relatively inexpensive, nondestructive, and fast method to measure the number of atoms in an ultrathin film. This study demonstrates that XRF is capable of detecting changes in the amounts of an element equivalent to a fraction of a monolayer for all elements examined and less than 1% of a monolayer for some elements. For films with thicknesses around a monolayer, the XRF intensity of the substrate before the film is deposited needs to be subtracted from the total signal of the film plus substrate to achieve this accuracy.

■ EXPERIMENTAL SECTION

Precursors were synthesized in a high-vacuum physical vapor deposition system, with depositions occurring at pressures below 5×10^{-7} Torr. Metals were deposited using electron beam guns, and selenium was deposited using an effusion cell.

A computer controlled pneumatic shutter system was used to control the sequence and thickness of the elemental layers. The rate of deposition and the thickness of each of the elemental layers deposited were measured and controlled using quartz crystal microbalances, with rates maintained at 0.1–0.3 Å/s at the substrate.

X-ray fluorescence data was collected using a Rigaku ZSX Primus II wavelength dispersive X-ray fluorescence spectrometer with a rhodium X-ray source. This instrument measures intensities of characteristic X-ray emission lines as a function of crystal angle. Samples were loaded onto a small metal puck with a 30 mm, 20 mm, or 10 mm diameter masking-frame. Incident X-rays were passed through either a 10 mm or 20 mm diaphragm before contacting the spinning sample in a vacuum. Fluoresced X-rays were reflected off selected crystals into a detector. Intensity was measured by integrating the area under the entire peak measured in intensity as a function of two-theta using MATLAB's cubic smoothing spline function (csaps) with the smoothing parameter set to zero smoothing (function value 1). The two-theta limits of integration were held constant. Data were also collected for substrates without any deposited film, referred to as blanks. The intensity data measured for the blanks was treated in the same manner as the deposited samples. The resulting integrated counts were subtracted from the integrated intensity of the coated substrates to correct for the background signal and any signal from the substrate itself.

X-ray diffraction (XRD) was used to characterize the structure of the samples that were subsequently analyzed by XRF. Low angle and specular XRD scans were collected using a Bruker d8-discover diffractometer. Grazing incidence inplane XRD scans were collected on a Rigaku Smartlab diffractometer. All diffraction patterns were collected with Cu $K\alpha$ radiation.

■ RESULTS AND DISCUSSION

The intensity of the XRF signal I_{ij} for a particular element i of interest in a film with a characteristic line j at wavelength λ_{ij} is given by 36,39

$$I_{ij} = \{K_j(\lambda_s)C_i/\mu_T(\lambda_{ij})\}\{1 - \exp[-\mu_T(\lambda_{ij})\rho d]\}$$
(1)

In eq 1, C_i is the mass fraction of element i in the film, ρ is the average film density, d is the film thickness, and $\mu_{\rm T}(\lambda_{ij})$ is the total mass absorption coefficient at λ_{ij} . $K_j(\lambda_s)$ is a product of many constants, including a constant representing the spectrometer geometry, the intensity of the excitation X-ray source, and the excitation probability for the characteristic line j under the spectrum of intensities of the excitation source. If the thickness of the analyzed film is thin enough, $\mu_{\rm T}(\lambda_{ij})\rho d$ becomes small, and for films within this thickness regime (defined in more detail later), the exponential can be expanded as a power series. If only the leading terms are kept, eq 1 simplifies to

$$I_{ij} = C_i K_j(\lambda_s) \rho d \tag{2}$$

For such thin films the intensity of the XRF signal is thus expected to be directly proportional to the product of C_i , ρ , and d, which is the number of atoms of element i in the area of the film probed. The deviation between eq 1 and eq 2 as a function of film thickness for a representative film is shown in Figure A in the Supporting Information.

To test the applicability of this approximation, a series of films with thicknesses below 120 nm containing a variety of elements with different elemental ratios were prepared using physical vapor deposition. Quartz crystal microbalances were used to measure the amount of material deposited onto the silicon substrates. Figure 1a,b and Figure B in the Supporting

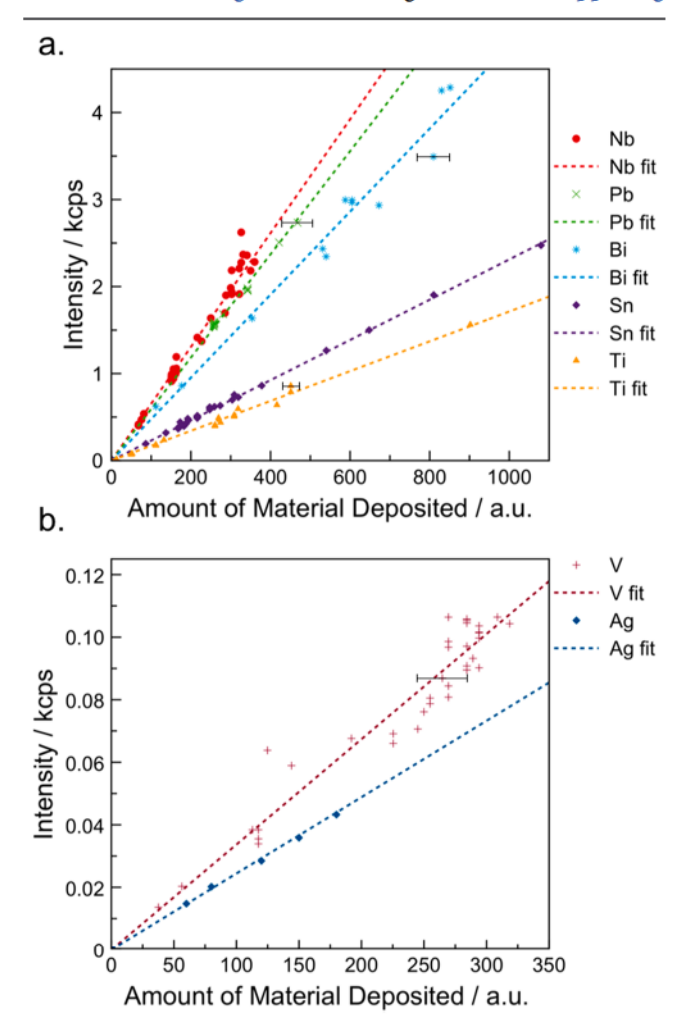


Figure 1. Change in the XRF intensity as a function of the thickness of material deposited as measured by quartz crystal monitors for a variety of different elements (shown with different colors and symbols). The error in the amount of material deposited for each element is shown for a single data point, and when error bars are absent the error is the size of the marker. The lines are fits assuming that the XRF intensity is directly proportional to the amount of material deposited. Slopes for each line can be found in Table 1.

Information each contain a graph of the background corrected intensity of the XRF signal as a function of the thickness of each element deposited. The intensity data for each element was found to be proportional to the amount of the element in the film. The linear relationship between intensity and amount of material indicates that the absorption of both the incident and fluorescence X-rays is negligible in these films. The greater the slope of the line, the more sensitivity there is to small changes in the amount of the element in the film. Table 1 summarizes the slopes and associated errors as well as the X-ray absorption line used for all of elements that were studied. Figure C in the Supporting Information explains how each line was chosen for each element in question.

Table 1. Slopes of the Lines in Figure 1 for Each Element along with the Fluorescence Line Used^a

element	line used	slope	maximum film thickness (nm)
Ag	$L\alpha$	0.00024(1)	150
Bi	$L\alpha$	0.00477(9)	1300
Mo	$L\alpha$	0.03019(9)	100
Nb	$L\alpha$	0.00653(6)	100
Pb	$M\alpha$	0.00592(4)	100
Se	$L\alpha$	0.00319(3)	50
Sn	$L\alpha$	0.00231(1)	200
Ti	$K\alpha$	0.00171(3)	200
V	$K\alpha$	0.000337(5)	250

^aThe maximum film thickness is the thickness where absorption reduces the intensity of fluorescence of the given element by 5%.

The spread of the data points about the linear relationship in Figure 1 results from several potential sources, including the limits of the reproducibility of the deposition process itself (for example the shape of the deposition plumes), limits to resolution of the quartz crystal monitors, and limits to the reproducibility of the XRF measurements. To assess the reproducibility of the XRF measurements, the XRF intensity of the same sample was measured repeatedly over a time period of 6 months, using a variety of sample masks of nominally the same size that define the sample size analyzed. The intensities for most elements studied were constant to less than a third of a percent. This suggests that the majority of the deviation in the plotted intensity versus amount deposited plots is due to errors in the amount of material deposited from either the crystal monitors or the deposition process itself.

The sensitivity of the XRF intensity to the amount of material deposited makes it a valuable tool to improve deposition reproducibility. For example, the amount of Se deposited on a sample was found to systematically increase with time when high melting point metals were evaporated in the same deposition even though the thicknesses deposited onto the quartz crystal microbalance was kept constant. The excess Se resulted from Se evaporating from chamber walls as they were heated by infrared radiation from the electron beam deposition. The sensitivity of the XRF data combined with tracking the data as a function of time and experimental conditions is a powerful tool to improve deposition processes.

The approximation that $\mu_T(\lambda_i)\rho d$ is small neglects absorption corrections to the measured fluorescence intensity. When $\mu_T(\lambda_i)\rho d = 0.1$, the difference between the intensities calculated with and without absorption corrections yields an error of ~5%. Absorption corrections become more important as the energy of the X-ray fluorescence line decreases as shown in Figures D, E, and F in the Supporting Information. 40,41 Table 1 contains estimates of the thickness where the error in neglecting absorption becomes 5%, assuming a film with a total mass absorption coefficient of $\sim 10^3$ cm²/g and a density of ~ 10 g/cm³. For most elements, this corresponds to a film that is more than 100 nm thick. While the exact thickness depends on the element being probed, the mass absorption coefficient of the matrix, and the density of the film, the approximation that $\mu_T(\lambda_i)\rho d$ is small is a conservative approximation for thicknesses less than 50 nm for most elements. Films below this thickness are common in many research projects and in many devices prepared by sequential deposition of layers. The Supporting Information contains calculations of the thickness value when the calculated intensity of the given material using

eq 2 is 5% higher than the intensity calculated for eq 1 for samples containing Bi, Pb, or Se in their matrix using $K\alpha$, $L\alpha$, and $M\alpha$ lines.

While quantifying the relative amount of an element in a film is valuable when monitoring a process, determining the number of atoms per unit area is significantly more valuable in many research applications. Unfortunately, $K(\lambda_s)$ is a product of many constants that are difficult to quantify or calculate, and both the average film density and thickness are generally difficult to experimentally determine. Our approach to quantifying the amount of material in a film per unit area is to synthesize standards where the number of atoms of each element per unit area can be calculated from diffraction data. Figure 2 contains representative X-ray reflectivity (XRR), specular XRD, and in-plane XRD scans of one of these films, a sample of [(PbSe)_{1,12}]₁[NbSe₂]₁. The Kiessig fringes in the XRR scan provide a measure of the smoothness of the film and allow the total thickness and the total number of repeats of the film to be calculated. The number of repeat units in the film is equal to the number of Kiessig fringes plus 2. The specular diffraction scan shows that the film is crystallographically aligned with the substrate and enables the c-axis lattice parameter to be determined. The value of the c-lattice parameter informs on how many of each layer type are in the repeat unit. The total thickness of the film divided by the caxis lattice parameter yields an integer, indicating that all of the film thickness comes from the crystalline material. Assuming there are no impurity phases present that are not evident in the diffraction scans, for example, an amorphous phase, the number of atoms of each element per unit area can be calulcated from the product of the number of crystallographically aligned unit cells obtained from the specular diffraction information and the number of atoms per unit cell from the structure solution divided by the area per unit cell obtained from the in-plane lattice parameters.

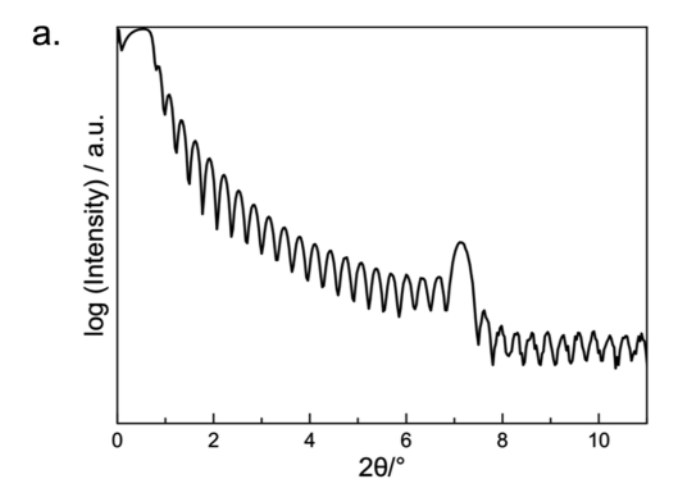
As an example, using the data in Figure 2, the formula to calculate atoms per unit area is given by

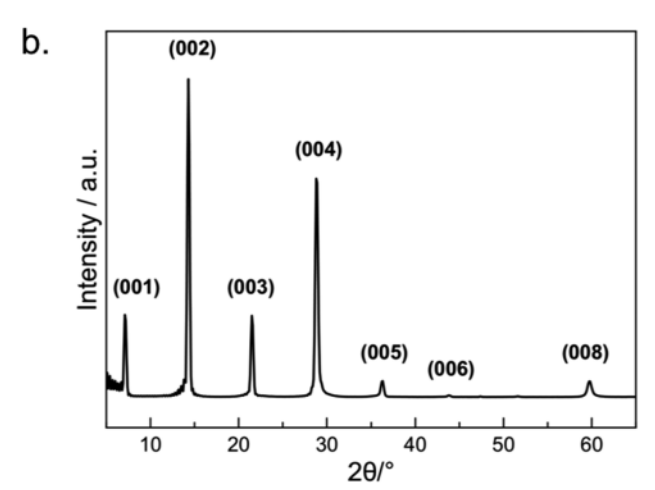
$$Total \frac{atoms}{A^2}$$

$$= \sum_{Constituent Layers} \left(\frac{\text{# of atoms per unit cell in basal plane}}{\text{area of the basal plane per unit cell}} \right) (\text{# of layers})$$
(3)

In Figure 2, the XRR pattern of $[(PbSe)_{1.12}]_1[NbSe_2]_1$ has 20 Kiessig fringes present between the critical angle and the first Bragg reflection, indicating that there are 22 repeat units of the $[(PbSe)_{1.12}]_1[NbSe_2]_1$ structure in the film. The total thickness of the film is obtained from the spacing between the Kiessig fringes. The specular diffraction pattern shown in the Figure 2b yields a *c*-axis lattice parameter of 12.39(2) Å which matches the targeted *c*-axis lattice parameter for a $[(PbSe)_{1.12}]_1[NbSe_2]_1$ heterostructure. Dividing the total thickness by the *c*-axis lattice parameter yields the number of repeating layers in the film, which in this case is 22, agreeing with the number of layers determined from the number of Kiessig fringes. Since the repeating unit contains one layer of PbSe and one layer of NbSe₂, the number of layers in eq 3 is 22 for both constituents.

In-plane XRD is used to determine the number of atoms and the area of the basal planes in each unit cell. All the reflections in the in-plane diffraction pattern (Figure 2c) can be indexed as hk0 reflections for PbSe and NbSe₂, consistent with the formation of a $[(PbSe)_{1,12}]_1[NbSe_2]_1$ heterostructure.⁴² The





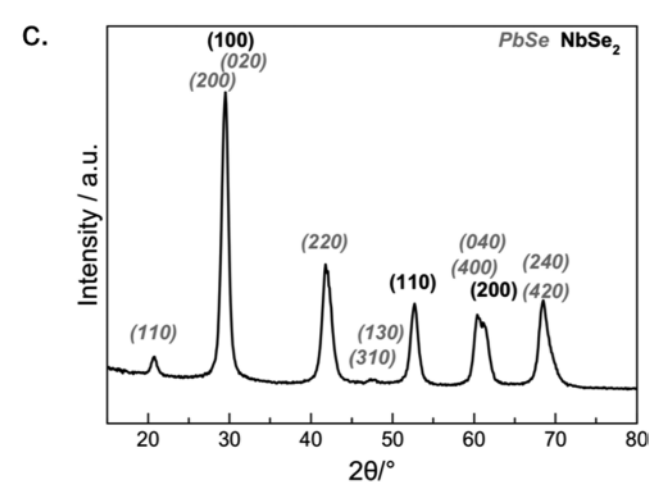


Figure 2. Three different diffraction scans of a $[(PbSe)_{1+\delta}]_1[NbSe_2]_1$ film. (a) XRR scan. (b) Specular XRD scan. (c) Grazing incidence inplane XRD scan. The crystallographic indices are given above each reflection and were used to determine the total film thickness from (a), the *c*-axis unit cell parameter from (b), and the in-plane unit cell parameters from (c).

indices are consistent with a rectangular basal plane for PbSe (distorted rock-salt structure) and a hexagonal basal plane for NbSe₂. The number of atoms per unit cell in the basal plane follow from the crystal structure of each constituent (4 Pb and 4 Se for PbSe and 1 Nb and 2 Se for NbSe₂). The indexed patterns are then used to calculate the *a*-lattice and *b*-lattice

parameters for the PbSe constituent (6.06 and 6.14 Å, respectively) and the *a*-lattice parameter for the NbSe₂ constituent (3.47 Å). The resulting basal plane areas for each constituent, assuming that they are stoichiometric, are 12.5 Å² for PbSe and 9.47 Å² for NbSe₂. Using this information, we calculate that the $[(PbSe)_{1.12}]_1[NbSe_2]_1$ film contains 2.37 Pb atoms/Å², 2.11 Nb atoms/Å² and 6.58 Se atoms/Å².

Figure 3 shows the XRF intensity for a number of different elements versus the calculated number of atoms of each element in a series of films containing a variety of different rock salt structured constituents and transition metal dichalcogenides that have diffraction data similar to that displayed in Figure 2. The data for each element is well described by

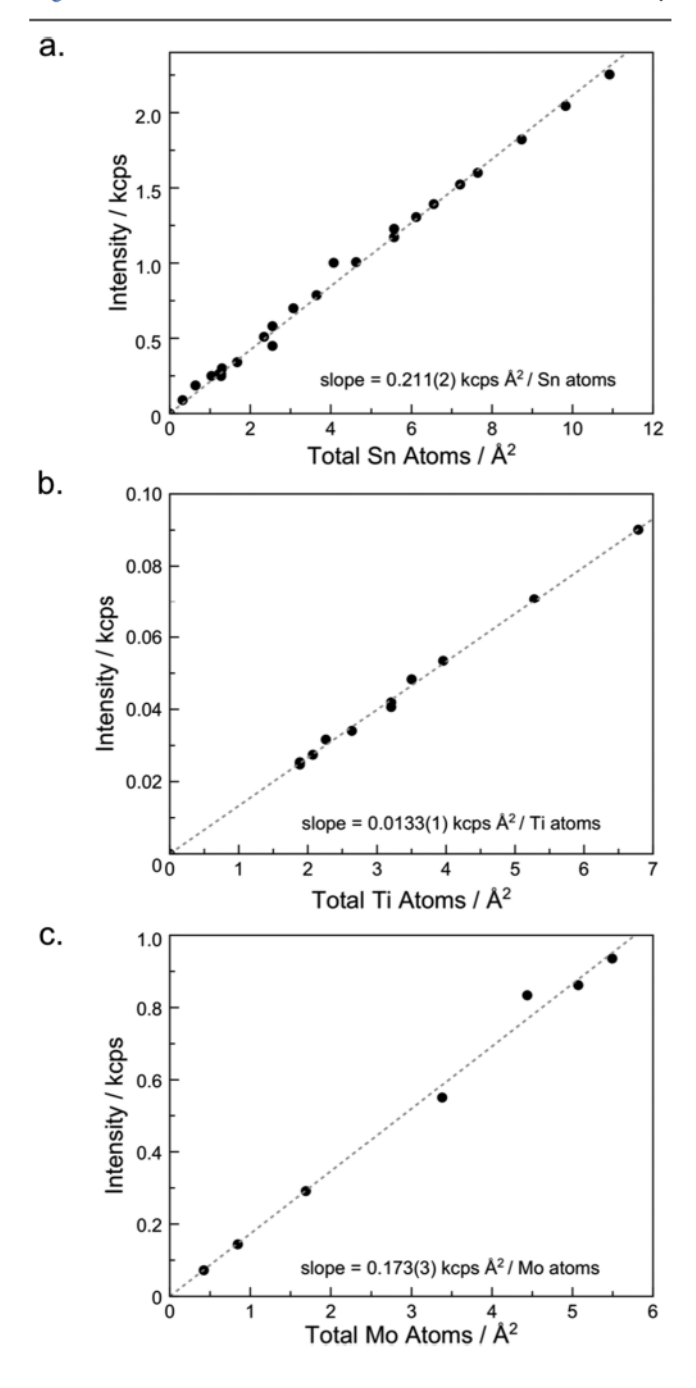


Figure 3. Graphs of the XRF intensity versus the number of atoms per unit area of several elements calculated from diffraction information such as that shown in Figure 2 for a number of different films.

straight lines through the origin, where the slopes provide the conversion factor between intensity and atoms per unit area. The Supporting Information contains data for other elements (Figure G), reinforcing that this is a reasonable approach to obtain the proportionality constant between the XRF intensity and number of atoms in the analytical volume. The largest error in this approach is the assumption that the films do not contain either significant defect densities or amorphous phases that are not evident in the diffraction scans. The observed linear behavior for films containing a variety of different constituents suggests that the approximation is valid, and using the slope averages this error over many samples. The graph for selenium (Figure 4) has the largest deviations. We believe

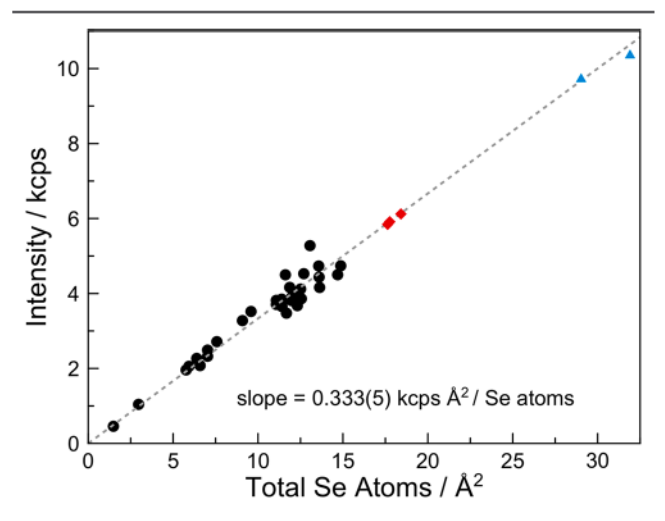


Figure 4. XRF intensity versus the total number of Se atoms per unit area determined from diffraction information (black), from films of SnSe₂ (red), and from films of TiSe₂ (blue). For the SnSe₂ and TiSe₂ films, the information in Figure 3 was used to determine the number of cation atoms in these films from the measured Sn and Ti XRF intensities. These values were then used to calculate the number of Se atoms in each of the films.

points above the line are the result of small amounts of amorphous Se in grain boundaries, inclusions, and on the surface of the films, which could be removed by additional annealing time. Points below the line are likely the result of Se loss due to annealing the samples for too long in an open system. The ability to accurately and nondestructively measure Se content will aid researchers in adjusting the annealing temperatures and times to obtain stoichiometric Se content.

Once the conversion factor is known for a particular element, the conversion factor for other elements can be determined by measuring XRF intensities of stoichiometric compounds that contain elements with known and unknown conversion factors. For example, to obtain the conversion factor for Se, XRF measurements on thin films with stoichiometric SnSe₂ can be used. The conversion factor of Se is then determined using the XRF intensities of Sn and Se, the known conversion factor of Sn (Figure 3), and the stoichiometry of the crystal. Figure 4 illustrates this process for three SnSe₂ and two TiSe₂ films, where the validity of this approach is confirmed by the consistency of the calculated conversion factor with that determined from crystal structure information as presented in Figure 3 for other elements.

While the number of atoms per unit area in a thin film via XRF can be determined with less than 1% error, the error increases as the amount of an element approaches zero, so

subtracting the background signal becomes more significant. Figure 5 shows the signal from the Sn $L\alpha$ emission line for a

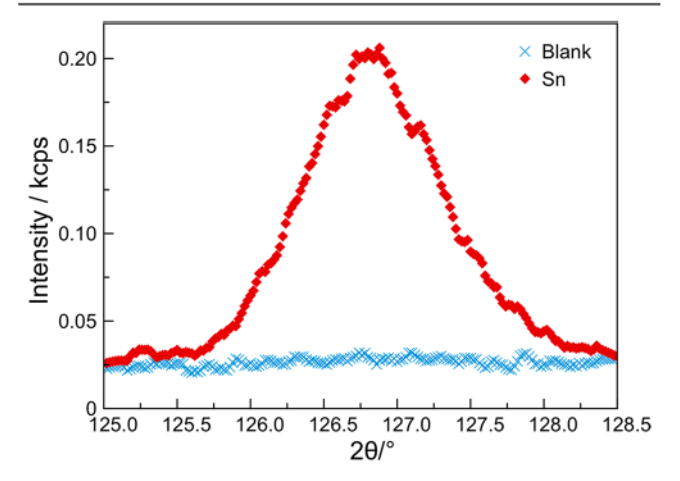


Figure 5. Sn–L α emission intensity from a film with 0.11 Sn/Å² and the blank Si substrate before deposition of Sn.

silicon substrate and the substrate with 0.11 atoms of Sn/Å² (\sim 140% of the amount of Sn in a single layer of SnSe₂)). The background intensity constitutes roughly 20% of the total intensity under the Sn L α background intensity correctly. For Sn films deposited on silicon substrates under these data collection times and conditions (less than an hour total scan time for both film and blank substrate), the error of the net intensity measurements in our instruments indicates that changes of less than 1% of a monolayer film of SnSe2 can be detected. The sensitivity of detecting small changes of an element depends on the change in intensity of the XRF signal for that element, which is proportional to the slope of the lines in Figure 1, and on the specific diffracting crystals and detectors used. For example, the intensity of the Pb emission from the M α line is about 10 times more intense per atom than the intensity of the Ti emission from the $K\alpha$ line in our instrument. Therefore, we can detect smaller changes in Pb atoms/Å² than Ti atoms/Å². Sensitivities for several elements based on the data collected in this study are given in Table 2.

Table 2. Sensitivity of the XRF Measurement for a Series of Elements as a Percent of a Monolayer of the Compound in Parentheses

element	sensitivity
Sn (SnSe)	>1%
Pb (PbSe)	>1%
Nb (NbSe ₂)	>1%
Mo (MoSe ₂)	2%
V (VSe ₂)	7%
Ti (TiSe ₂)	10%

For ultrathin films (a monolayer or less), the ability to subtract the background intensity accurately and reproducibly is obviously critical, making the choice of the emission line an important factor. Figure C in the Supporting Information illustrates this point, showing the measured intensity of a Pb-containing sample and its blank substrate for three different emission lines, the L α , the L β ₁, and the M α . While the signal intensity is largest for the L α emission line, the low and

constant intensity measured on the blank substrate for the $M\alpha$ line makes it the preferred emission line.

The ability to quickly measure the number of atoms per unit area of each element in a film enables films to be prepared with a precise number of unit cells such as that shown in Figure 2. To demonstrate this, we used a film with eight elemental Mo and Se layers that were sequentially deposited onto a room temperature silicon substrate, with each pair containing the appropriate amount of these elements per unit area to form a single crystalline MoSe₂ layer. After annealing at 650 °C, a variety of diffraction and reflectivity scans were collected. The XRR scan in Figure 6 is that expected for a film containing 8

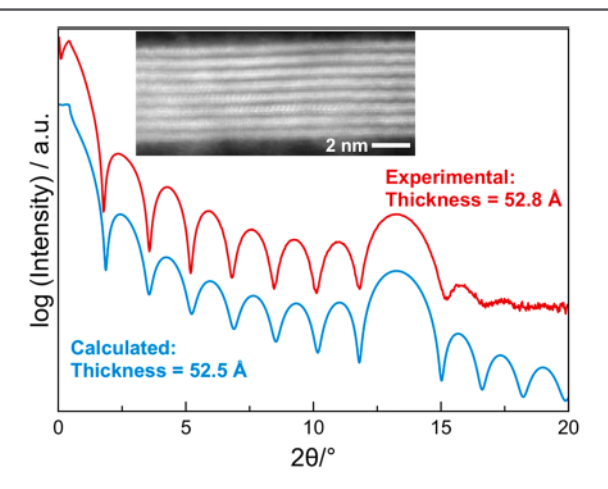


Figure 6. Measured and calculated XRR patterns of an 8-layer MoSe₂ film showing the application of this XRF method to prepare films containing a finite number of layers. The inset HAADF-STEM image shows further evidence of the formation of 8 MoSe₂ layers.

identical layers, with a thickness consistent with 8 MoSe₂ trilayers. The high angle annular dark field scanning transmission electron microscopy (HAADF-STEM) cross-section image of this sample, also shown in Figure 6, is consistent with the XRR scan. The specular diffraction pattern contains only four broad 00l reflections, indicating that the MoSe₂ is crystallographically aligned with the substrate yielding a c-axis lattice parameter of 6.53(1) Å, consistent with the literature value of 6.46 Å. The in-plane diffraction pattern contains only hk0 reflections, from which an a-axis lattice parameter of 3.27(3) Å was calculated. This is in good agreement with that previously reported for MoSe₂ (3.31 Å). 43

CONCLUSION

XRF is a sensitive and precise probe of the number of atoms per unit area of select elements in thin film samples. If films are thin enough, absorption corrections can be ignored, and the matrix has minimal impact on fluorescence intensity. The proportionality factor between intensity and the number of atoms of each element per unit area was determined using diffraction data from smooth, crystallographically aligned thin films that are an integral number of unit cells in thickness. The sensitivity of this approach enables less than 1% of a monolayer to be quantified.

ASSOCIATED CONTENT

Supporting Information

The Supporting Information is available free of charge on the ACS Publications website at DOI: 10.1021/acs.chemmater.8b02591.

Graph of XRF intensity against film thickness to show deviation of thick samples from linear behavior, plot of intensity versus amount of material deposited for Mo, different Pb X-ray emission lines for a sample and a blank substrate, calculated X-ray emission lines for Bi, Pb, and Se vs film thickness, and calibration plots of intensity vs atom per square angstrom for Bi, Nb, Pb, and Se (PDF)

AUTHOR INFORMATION

Corresponding Author

*(D.C.J.) E-mail: davej@uoregon.edu.

ORCID ®

Danielle M. Hamann: 0000-0002-9262-1060 Alexander C. Lygo: 0000-0003-1762-244X Suzannah R. Wood: 0000-0002-7208-7681 Marco Esters: 0000-0002-8793-2200 David C. Johnson: 0000-0002-1118-0997

Present Addresses

^T(S.R.W.) XTD-IDA, Los Alamos National Laboratory, Los Alamos, New Mexico 87545, United States.

§(M.E.) Center for Materials Genomics, Duke University, Durham, North Carolina 27708, United States.

Author Contributions

The manuscript was written through contributions of all authors.

Notes

The authors declare no competing financial interest.

ACKNOWLEDGMENTS

A.C.L. acknowledges support from the University of Oregon Office of the Vice President of Research and Innovation (VPRI) and the Presidential Undergraduate Research Scholarship (PURS). This material is based upon work supported by the National Science Foundation Graduate Research Fellowship Program under Grant No. 1309047. The authors acknowledge support from the National Science Foundation under Grant DMR-1710214. We would like to acknowledge the Center for Advanced Materials Characterization in Oregon (CAMCOR) at the University of Oregon.

ABBREVIATIONS

XRF, X-ray fluorescence; XRR, X-ray reflectivity; XRD, X-ray diffraction; HAADF-STEM, high angle annular dark field scanning transmission electron microscopy

■ REFERENCES

- (1) Novoselov, K. S.; Geim, A. K.; Morozov, S. V.; Jiang, D.; Zhang, Y.; Dubonos, S. V.; Grigorieva, I. V.; Firsov, A. A. Electric Field Effect in Atomically Thin Carbon Films. *Science* 2004, 306, 666–669.
- (2) Novoselov, K. S. Nobel Lecture: Graphene: Materials in the Flatland. Rev. Mod. Phys. 2011, 83, 837-849.
- (3) Grubišić Čabo, A.; Miwa, J. A.; Grønborg, S. S.; Riley, J. M.; Johannsen, J. C.; Cacho, C.; Alexander, O.; Chapman, R. T.; Springate, E.; Grioni, M.; Lauritsen, J. V.; King, P. D. C.; Hofmann,

P.; Ulstrup, S. Observation of Ultrafast Free Carrier Dynamics in Single Layer MoS₂. Nano Lett. 2015, 15, 5883–5887.

- (4) Bruix, A.; Miwa, J. A.; Hauptmann, N.; Wegner, D.; Ulstrup, S.; Grønborg, S. S.; Sanders, C. E.; Dendzik, M.; Grubišić Čabo, A.; Bianchi, M.; Lauritsen, J. V.; Khajetoorians, A. A.; Hammer, B.; Hofmann. Single-Layer MoS₂ on Au(111): Band Gap Renormalization and Substrate Interaction. *Phys. Rev. B: Condens. Matter Mater. Phys.* 2016, 93, 165422.
- (5) Geim, A. K. Nobel Lecture: Random Walk to Graphene. Rev. Mod. Phys. 2011, 83, 851-862.
- (6) Hamann, D. M.; Hadland, E. C.; Johnson, D. C. Heterostructures Containing Dichalcogenides-New Materials with Predictable Nanoarchitectures and Novel Emergent Properties. *Semicond. Sci. Technol.* 2017, 32, 093004.
- (7) Jariwala, D.; Marks, T. J.; Hersam, M. C. Mixed-Dimensional van Der Waals Heterostructures. *Nat. Mater.* 2017, 16, 170–181.
- (8) Mak, K. F.; Lee, C.; Hone, J.; Shan, J.; Heinz, T. F. Atomically Thin MoS₂: A New Direct-Gap Semiconductor. *Phys. Rev. Lett.* 2010, 105. 136805–136805.
- (9) Zhao, W.; Ghorannevis, Z.; Chu, L.; Toh, M.; Kloc, C.; Tan, P. H.; Eda, G. Evolution of Electronic Structure in Atomically Thin Sheets of WS₂ and WSe₂. ACS Nano 2013, 7, 791–797.
- (10) Komsa, H. P.; Krasheninnikov, A. V. Electronic Structures and Optical Properties of Realistic Transition Metal Dichalcogenide Heterostructures from First Principles. *Phys. Rev. B: Condens. Matter Mater. Phys.* 2013, 88, 085318.
- (11) Ulstrup, S.; Čabo, A. G.; Miwa, J. A.; Riley, J. M.; Grønborg, S. S.; Johannsen, J. C.; Cacho, C.; Alexander, O.; Chapman, R. T.; Springate, E.; Bianchi, M.; Dendzik, M.; Lauritsen, J. V.; King, P. D. C.; Hofmann, P. Ultrafast Band Structure Control of a Two-Dimensional Heterostructure. ACS Nano 2016, 10, 6315–6322.
- (12) Ugeda, M. M.; Bradley, A. J.; Shi, S. F.; da Jornada, F. H.; Zhang, Y.; Qiu, D. Y.; Ruan, W.; Mo, S. K.; Hussain, Z.; Shen, Z. X.; Wang, F.; Louie, S. G.; Crommie, M. F. Giant Bandgap Renormalization and Excitonic Effects in a Monolayer Transition Metal Dichalcogenide Semiconductor. *Nat. Mater.* 2014, 13, 1091–1095
- (13) Xie, Y.; Wang, Z.; Zhan, Y.; Zhang, P.; Wu, R.; Jiang, T.; Wu, S.; Wang, H.; Zhao, Y.; Nan, T.; Ma, X. Controllable Growth of Monolayer MoS₂ by Chemical Vapor Deposition via Close MoO₂ Precursor for Electrical and Optical Applications. *Nanotechnology* 2017, 28, 084001.
- (14) Shaw, J. C.; Zhou, H.; Chen, Y.; Weiss, N. O.; Liu, Y.; Huang, Y.; Duan, X. Chemical Vapor Deposition Growth of Monolayer MoSe₂ Nanosheets. *Nano Res.* 2014, 7, 511–517.
- (15) Schmidt, H.; Wang, S.; Chu, L.; Toh, M.; Kumar, R.; Zhao, W.; Castro Neto, A. H.; Martin, J.; Adam, S.; Özyilmaz, B.; Eda, G. Transport Properties of Monolayer MoS₂ Grown by Chemical Vapor Deposition. *Nano Lett.* 2014, 14, 1909–1913.
- (16) Shang, S. L.; Lindwall, G.; Wang, Y.; Redwing, J. M.; Anderson, T.; Liu, Z. K. Lateral Versus Vertical Growth of Two-Dimensional Layered Transition-Metal Dichalcogenides: Thermodynamic Insight into MoS₂. Nano Lett. 2016, 16, 5742–5750.
- (17) Ling, X.; Lee, Y. H.; Lin, Y.; Fang, W.; Yu, L.; Dresselhaus, M. S.; Kong, J. Role of the Seeding Promoter in MoS₂ Growth by Chemical Vapor Deposition. *Nano Lett.* 2014, 14, 464–472.
- (18) Tsai, M. L.; Su, S. H.; Chang, J. K.; Tsai, D. S.; Chen, C. H.; Wu, C. I.; Li, L. J.; Chen, L. J.; He, J. H. Monolayer MoS₂ Heterojunction Solar Cells. *ACS Nano* 2014, *8*, 8317–8322.
- (19) Cain, J. D.; Shi, F.; Wu, J.; Dravid, V. P. Growth Mechanism of Transition Metal Dichalcogenide Monolayers: The Role of Self-Seeding Fullerene Nuclei. ACS Nano 2016, 10, 5440-5445.
- (20) Kang, K.; Xie, S.; Huang, L.; Han, Y.; Huang, P. Y.; Mak, K. F.; Kim, C. J.; Muller, D.; Park, J. High-Mobility Three-Atom-Thick Semiconducting Films with Wafer-Scale Homogeneity. *Nature* 2015, 520, 656–660.
- (21) Ji, Q.; Zhang, Y.; Gao, T.; Zhang, Y.; Ma, D.; Liu, M.; Chen, Y.; Qiao, X.; Tan, P. H.; Kan, M.; Feng, J.; Sun, Q.; Liu, Z. Epitaxial

Monolayer MoS_2 on Mica with Novel Photoluminescence. *Nano Lett.* 2013, 13, 3870–3877.

- (22) Lee, Y. H.; Zhang, X. Q.; Zhang, W.; Chang, M. T.; Lin, C. T.; Chang, K. Di; Yu, Y. C.; Wang, J. T. W.; Chang, C. S.; Li, L. J.; Lin, T. W. Synthesis of Large-Area MoS₂ Atomic Layers with Chemical Vapor Deposition. *Adv. Mater.* 2012, 24, 2320–2325.
- (23) Najmaei, S.; Liu, Z.; Zhou, W.; Zou, X.; Shi, G.; Lei, S.; Yakobson, B. I.; Idrobo, J. C.; Ajayan, P. M.; Lou, J. Vapour Phase Growth and Grain Boundary Structure of Molybdenum Disulphide Atomic Layers. *Nat. Mater.* 2013, 12, 754–759.
- (24) Govind Rajan, A.; Warner, J. H.; Blankschtein, D.; Strano, M. S. Generalized Mechanistic Model for the Chemical Vapor Deposition of 2D Transition Metal Dichalcogenide Monolayers. *ACS Nano* 2016, 10, 4330–4344.
- (25) Wang, S.; Rong, Y.; Fan, Y.; Pacios, M.; Bhaskaran, H.; He, K.; Warner, J. H. Shape Evolution of Monolayer MoS₂ Crystals Grown by Chemical Vapor Deposition. *Chem. Mater.* 2014, 26, 6371–6379.
- (26) Liu, B.; Fathi, M.; Chen, L.; Abbas, A.; Ma, Y.; Zhou, C. Chemical Vapor Deposition Growth of Monolayer WSe₂ with Tunable Device Characteristics and Growth Mechanism Study. ACS Nano 2015, 9, 6119–6127.
- (27) Dumcenco, D. O.; Kobayashi, H.; Liu, Z.; Huang, Y. S.; Suenaga, K. Visualization and Quantification of Transition Metal Atomic Mixing in Mo_{1-x}W_xS₂ Single Layers. *Nat. Commun.* 2013, 4, 1351
- (28) Matetskiy, A. V.; Kibirev, I. A.; Hirahara, T.; Hasegawa, S.; Zotov, A. V.; Saranin, A. A. Direct Observation of a Gap Opening in Topological Interface States of MnSe/Bi₂Se₃ Heterostructure. *Appl. Phys. Lett.* 2015, 107, 091604.
- (29) Hirahara, T.; Eremeev, S. V.; Shirasawa, T.; Okuyama, Y.; Kubo, T.; Nakanishi, R.; Akiyama, R.; Takayama, A.; Hajiri, T.; Ideta, S.; Matsunami, M.; Sumida, K.; Miyamoto, K.; Takagi, Y.; Tanaka, K.; Okuda, T.; Yokoyama, T.; Kimura, S.; Hasegawa, S.; Chulkov, E. V. Large-Gap Magnetic Topological Heterostructure Formed by Subsurface Incorporation of a Ferromagnetic Layer. *Nano Lett.* 2017, 17, 3493–3500.
- (30) Ohlhausen, J. A.; Zavadil, K. R. Time-of-Flight Secondary Ion Mass Spectrometry Measurements of a Fluorocarbon-Based Self-Assembled Monolayer on Si. J. Vac. Sci. Technol., A 2006, 24, 1172—1178.
- (31) Laguitton, D.; Parrish, W. Simultaneous Determination of Composition and Mass Thickness of Thin Films by Quantitative X-Ray Fluorescence Analysis. *Anal. Chem.* 1977, 49, 1152–1156.
- (32) Remmel, T.; Werho, D. Development of an Xrf Metrology Method for Composition and Thickness of Barium Strontium Titanate Thin Films. *Adv. X-ray Anal.* 2000, 42, 99–108.
- (33) Van De Weijer, P.; De Boer, D. K. G. Elemental Analysis of Thin Layers by X-Rays. *Philips J. Res.* 1993, 47, 247–262.
- (34) Sitko, R.; Zawisz, B. Quantification in X-Ray Fluorescence Spectrometry. In X-Ray Spectroscopy; InTech: 2012.
- (35) Vrielink, J. A. M.; Tiggelaar, R. M.; Gardeniers, J. G. E.; Lefferts, L. Applicability of X-Ray Fluorescence Spectroscopy as Method to Determine Thickness and Composition of Stacks of Metal Thin Films: A Comparison with Imaging and Profilometry. *Thin Solid Films* 2012, 520, 1740–1744.
- (36) Klenk, M.; Schenker, O.; Probst, U.; Bucher, E. X-Ray Fluorescence Measurements of Thin Film Chalcopyrite Solar Cells. Sol. Energy Mater. Sol. Cells 1999, 58, 299–319.
- (37) Esters, M. Deposition Software for the Inficon IC6 Deposition Controller: https://github.com/marcoesters/deposition_ic6.
- (38) Fister, L.; Li, X.; McConnell, J.; Novet, T.; Johnson, D. C. Deposition System for the Synthesis of Modulated, Ultrathin-film Composites. J. Vac. Sci. Technol., A 1993, 11, 3014–3019.
- (39) Sherman, J. The Theoretical Derivation of Fluorescent X-Ray Intensities from Mixtures. *Spectrochim. Acta* 1955, 7, 283-306.
- (40) Sauter, F. Über Den Atomaren Photoeffekt Bei Großer Härte Der Anregenden Strahlung. Ann. Phys. 1931, 401, 217.

(41) Sauter, F. Über Den Atomaren Photoeffekt in Der K-Schale Nach Der Relativistischen Wellenmechanik Diracs. *Ann. Phys.* 1931, 403, 454.

- (42) Alemayehu, M. B.; Mitchson, G.; Ditto, J.; Hanken, B. E.; Asta, M.; Johnson, D. C. Charge Transfer between PbSe and NbSe₂ in [(PbSe)_{1.14]m} (NbSe₂)₁ Ferecrystalline Compounds. *Chem. Mater.* 2014, 26 (5), 1859–1866.
- (43) Bronsema, K. D.; De Boer, J. L.; Jellinek, F. On the Structure of Molybdenum Diselenide and Disulfide. *Z. Anorg. Allg. Chem.* 1986, 540, 15–17.